3D-FDTD-PML ANALYSIS OF LEFT-HANDED METAMATERIALS

Davi Correia and Jian-Ming Jin
Center of Computational Electromagnetics (CCEM)
Dept. of Electrical and Computer Engineering
University of Illinois at Urbana-Champaign (UIUC)
Illinois

Received 22 July 2003

ABSTRACT: *The increasing interest in negative-index metamaterials requires a formulation capable of a full analysis of wave propagation in such materials. Since two-dimensional (2D) problems have been largely explored in the literature, the natural step is a three-dimensional (3D) formulation of a metamaterial. In this work, we present a simulation of a left-handed metamaterial using the finite-difference time-domain (FDTD) method in conjunction with perfectly matched layers (PMLs). First, we develop a PML to work with a Drude medium model. Then we apply our formulation to a 3D domain and compare our results with 2D problems. Finally, we simulate a dipole on the top of a metamaterial slab, presenting the field distribution in three different directions.* © 2004 Wiley Periodicals, Inc. Microwave Opt Technol Lett 40: 201–205, 2004; Published online in Wiley InterScience (www.interscience.wiley.com). DOI 10.1002/mop.11328

Key words: *left-handed metamaterials; negative index of refraction; 3D-FDTD method; PML*

1. INTRODUCTION

Left-handed metamaterials (LHMs) form a group of man-made materials that possess non-naturally occurring behavior. Their main characteristic is having both permeability and permittivity negative ($\mu < 0$, $\varepsilon < 0$). Remarkably, the direction of wave propagation $\mathbf{k}$ and the direction of the Poynting vector $\mathbf{S}$ are anti-parallel in this case. The theoretical behavior of wave propagation was first studied by Veselago [1]. The approach is quite simple. Starting from Maxwell's equations

$$\nabla \times \mathbf{E} = -j\omega\mu\mathbf{H}, \quad \nabla \times \mathbf{H} = j\omega\varepsilon\mathbf{E},$$

one can easily conclude that

$$\mathbf{k} \times \mathbf{E} = \omega\mu\mathbf{H}, \quad \mathbf{k} \times \mathbf{H} = -\omega\varepsilon\mathbf{E}, \tag{1}$$

assuming wave propagation in the form $e^{-j\mathbf{k}\cdot\mathbf{r}}$, where $\mathbf{k}$ is the propagation direction.

From Eq. (1) we can see that the triad formed by $\mathbf{E}$, $\mathbf{H}$, and $\mathbf{k}$ can have different behavior, depending on the sign of ε and μ. If $\varepsilon > 0$ and $\mu > 0$, then the direction of $\mathbf{S} = 1/2\ \mathbf{E} \times \mathbf{H}$ and $\mathbf{k}$ would be the same and hence the phase velocity and Poynting vector would point in the same direction. On the other hand, if $\varepsilon < 0$ and $\mu < 0$, they would have opposite sign. Such a medium would, among other things, have a negative index of refraction, accordingly to Veselago.

Thirty years after Veselago's work, Pendry et al. suggested (separately) two types of artificial materials with $\varepsilon < 0$ [2] and $\mu < 0$ [3]. Even though Pendry's idea was, at first, to use the new proposed materials for nonlinear phenomena, Shelby et al. [4] used his results to obtain what Veselago had predicted. They claimed to have experimentally obtained the negative index of refraction. This result was doubted by Valanju et al. [5], who stated that the angular intensity profile interpretation in [4] is a near-field effect. Valanju et al. also doubted, together with several other authors [6], the perfect lens suggested by Pendry [7], where he stated that perfect lens could be obtained using a metamaterial slab.

Ziolkowski et al. [8] has enlivened the discussion by numerical simulation means. He chose the finite-difference time-domain method (FDTD) to solve Maxwell's equations directly, without any assumption on the sign of the refractive index or the direction of wave propagation inside the LHM slab. Our goal is to increase the analysis capability by adding the perfectly matched layers (PMLs) formulation to Ziolkowski's approach, thus reducing the requirements for the computational domain, and simulating three-dimensional (3D) problems to enable the analysis of wave propagation in space.

2. FORMULATION

The formulation used to simulate wave propagation inside an LHM follows the one proposed by Ziolkowski et al. in [8, 9]. There, the authors developed the idea of the Drude medium used to simulate the negative μ and ε. Note that by simply imposing μ and ε negative inside the slab would produce an unstable simulation, since the field at the interface, for a matched case, would blow up. Hence, the Drude medium approach is more general and can be applied to both matched and unmatched interfaces.

To show how the instability would arise, we take Maxwell's equations for the two-dimensional (2D) TM case, for example,

$$\varepsilon \frac{\partial E_z}{\partial t} = \frac{\partial H_y}{\partial x} - \frac{\partial H_x}{\partial y} - J_z, \quad \mu \frac{\partial H_x}{\partial t} = -\frac{\partial E_z}{\partial y}, \quad \mu \frac{\partial H_y}{\partial t} = \frac{\partial E_z}{\partial x}, \tag{2}$$

and using Yee's standard algorithm [10], one can easily see that if H_x is at the interface, for example, to update its value one would have to take the average of μ from each side of the interface, given by

$$H_{xi,j+1}^{l+1} = H_{xi,j+1}^{l} - \frac{\Delta t}{\Delta y \times \mu_{\text{av}}}[E_{zi,j+1}^{l+1/2} - E_{zi,j}^{l+1/2}],$$

where the superscript l refers to the time step, and the subscripts i and j refer to the x and y directions, respectively. For the case with a matched interface ($\mu_1 = -\mu_2$, $\varepsilon_1 = -\varepsilon_2$), the average of the values would yield to $\mu_{\text{av}} = 0$, which would result in an unstable situation. The same problem occurs with E_z and H_y at the interface.

To avoid such instability, we set the negative values of μ and ε indirectly, using the Drude model [8]. First, let μ and ε be modeled by the following expressions:

$$\varepsilon = \varepsilon_0\left(1 - \frac{\omega_p^2}{\omega^2}\right), \quad \mu = \mu_0\left(1 - \frac{\omega_p^2}{\omega^2}\right), \tag{3}$$

with ω_p being the material's resonant frequency. Note that these expressions are similar to the ones previously used to characterize LHM [2–4, 7]. If we want to simulate $\varepsilon_r = \mu_r = -1$, for example, we simply choose $\omega_p = \sqrt{2}\omega$.

Substituting those expressions into Maxwell's equations in the frequency domain, we obtain

$$\mu_0 j\omega H_x + K_x = \frac{\partial E_y}{\partial z} - \frac{\partial E_z}{\partial y}, \quad \mu_0 j\omega H_y + K_y = \frac{\partial E_z}{\partial x} - \frac{\partial E_x}{\partial z},$$

This work was partially supported by the Brazilian Educational Agency CAPES, BEX 118401-6

$$\mu_0 j\omega H_z + K_z = \frac{\partial E_x}{\partial y} - \frac{\partial E_y}{\partial x}, \quad \varepsilon_0 j\omega E_x + J_x = \frac{\partial H_z}{\partial y} - \frac{\partial H_y}{\partial z},$$

$$\varepsilon_0 j\omega E_y + J_y = \frac{\partial H_x}{\partial z} - \frac{\partial H_z}{\partial x}, \varepsilon_0 j\omega E_z + J_z = \frac{\partial H_y}{\partial x} - \frac{\partial H_x}{\partial y},$$

with

$$K_x = -j\mu_0 \frac{\omega_p^2}{\omega} H_x, \quad K_y = -j\mu_0 \frac{\omega_p^2}{\omega} H_y,$$

$$K_z = -j\mu_0 \frac{\omega_p^2}{\omega} H_z, \quad J_x = -j\varepsilon_0 \frac{\omega_p^2}{\omega} E_x,$$

$$J_y = -j\varepsilon_0 \frac{\omega_p^2}{\omega} E_y, \quad J_z = -j\varepsilon_0 \frac{\omega_p^2}{\omega} E_z.$$

In the time domain, we finally have

$$\mu_0 \frac{\partial H_x}{\partial t} + K_x = \frac{\partial E_y}{\partial z} - \frac{\partial E_z}{\partial y}, \quad \mu_0 \frac{\partial H_y}{\partial t} + K_y = \frac{\partial E_z}{\partial x} - \frac{\partial E_x}{\partial z},$$

$$\mu_0 \frac{\partial H_z}{\partial t} + K_z = \frac{\partial E_x}{\partial y} - \frac{\partial E_y}{\partial x}, \quad \varepsilon_0 \frac{\partial E_x}{\partial t} + J_x = \frac{\partial H_z}{\partial y} - \frac{\partial H_y}{\partial z},$$

$$\varepsilon_0 \frac{\partial E_y}{\partial t} + J_y = \frac{\partial H_x}{\partial z} - \frac{\partial H_z}{\partial x}, \quad \varepsilon_0 \frac{\partial E_z}{\partial t} + J_z = \frac{\partial H_y}{\partial x} - \frac{\partial H_x}{\partial y},$$

$$\frac{\partial K_x}{\partial t} = \mu_0 \omega_p^2 H_x, \quad \frac{\partial K_y}{\partial t} = \mu_0 \omega_p^2 H_y,$$

$$\frac{\partial K_z}{\partial t} = \mu_0 \omega_p^2 H_z, \quad \frac{\partial J_x}{\partial t} = \varepsilon_0 \omega_p^2 E_x,$$

$$\frac{\partial J_y}{\partial t} = \varepsilon_0 \omega_p^2 E_y, \quad \frac{\partial J_z}{\partial t} = \varepsilon_0 \omega_p^2 E_z.$$

Note that with this new approach, we avoid the instability issue present when setting directly $\mu < 0$ and $\varepsilon < 0$. The application of Yee's algorithm is then straightforward, with J_x, K_x, J_y, K_y, J_z, and K_z being updated in each time step, as the E and H fields.

2.1. PML in a Drude Medium

Contrary to the two-time-derivative Lorentz material absorbing boundary condition employed to terminate the grid in [8], we decided to use the split-PML proposed by Berenger [11]. To use Berenger's PML, we split each field component into two components. To illustrate the procedure, we show how it is done for the first equation. The remaining equations follow the same process. To use Belenger's PML, we start with Maxwell's equations:

$$\left(1 - \frac{\omega_p^2}{\omega^2}\right) \mu_0 j\omega \mathbf{H}_{sx} + \sigma_x \frac{\mu}{\varepsilon} \mathbf{H}_{sx} = -\frac{\partial}{\partial x} \hat{x} \times \mathbf{E},$$

$$\left(1 - \frac{\omega_p^2}{\omega^2}\right) \mu_0 j\omega \mathbf{H}_{sy} + \sigma_y \frac{\mu}{\varepsilon} \mathbf{H}_{sy} = -\frac{\partial}{\partial y} \hat{y} \times \mathbf{E},$$

$$\left(1 - \frac{\omega_p^2}{\omega^2}\right) \mu_0 j\omega \mathbf{H}_{sz} + \sigma_z \frac{\mu}{\varepsilon} \mathbf{H}_{sz} = -\frac{\partial}{\partial z} \hat{z} \times \mathbf{E},$$

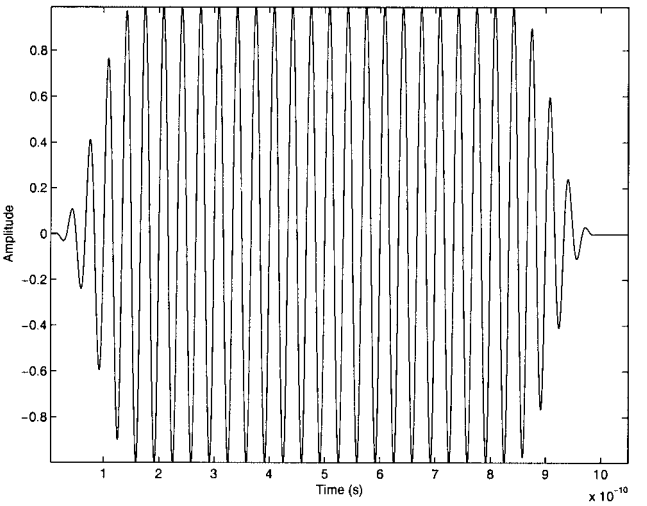

(a)

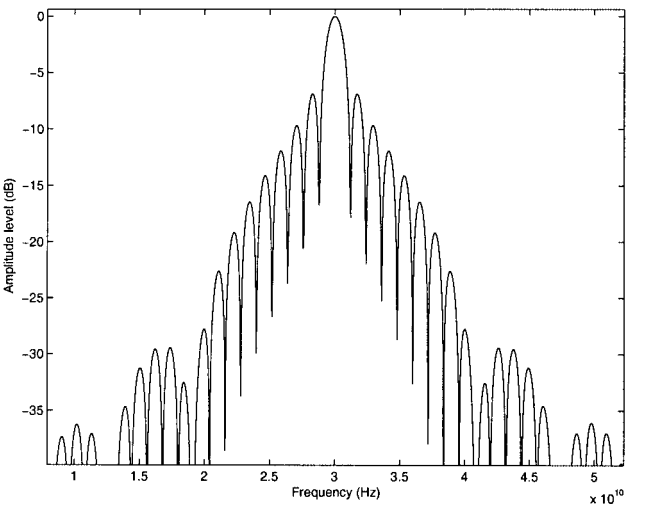

(b)

Figure 1 Excitation corresponding to (6) with $m = 5$, $n = 20$, and $\omega_0 = 2\pi \times 30 \times 10^9$ rad/s; (a) as a function of time; (b) its frequency components

$$\left(1 - \frac{\omega_p^2}{\omega^2}\right) \varepsilon_0 j\omega \mathbf{E}_{sx} + \sigma_x \mathbf{E}_{sx} = \frac{\partial}{\partial x} \hat{x} \times \mathbf{H},$$

$$\left(1 - \frac{\omega_p^2}{\omega^2}\right) \varepsilon_0 j\omega \mathbf{E}_{sy} + \sigma_y \mathbf{E}_{sy} = \frac{\partial}{\partial y} \hat{y} \times \mathbf{H},$$

$$\left(1 - \frac{\omega_p^2}{\omega^2}\right) \varepsilon_0 j\omega \mathbf{E}_{sz} + \sigma_z \mathbf{E}_{sz} = \frac{\partial}{\partial z} \hat{z} \times \mathbf{H}. \quad (4)$$

Equation (4) is first written as

$$\mu_0 j\omega \mathbf{H}_{sx} + \sigma_x \frac{\mu}{\varepsilon} \mathbf{H}_{sx} = -\frac{\partial}{\partial x} [\hat{z} E_y - \hat{y} E_z] - \mathbf{K}_{sx},$$

$$\mathbf{K}_{sx} = -\frac{\omega_p^2}{\omega} \mu_0 j \mathbf{H}_{sx}.$$

When these two equations are splitted into two components, we obtain

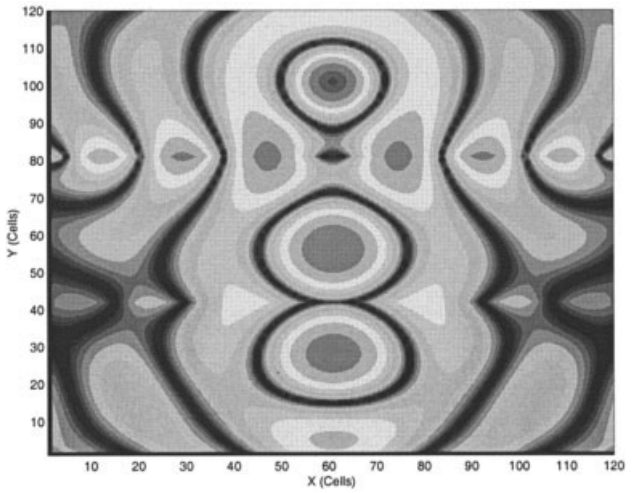

Figure 2 E_z-field intensity distribution at time $t = 1250\Delta t$ for $\omega_p = 266.6 \times 10^{11}$ rad/s

$$\mu_0 j\omega H_{sxz} + \sigma_x \frac{\mu}{\varepsilon} H_{sxz} = -\frac{\partial E_y}{\partial x} - K_{sxz},$$

$$\mu_0 j\omega H_{sxy} + \sigma_x \frac{\mu}{\varepsilon} H_{sxy} = \frac{\partial E_z}{\partial x} - K_{sxy},$$

$$j\omega K_{sxz} = \omega_p^2 \mu_0 H_{sxz}, \quad j\omega K_{sxy} = \omega_p^2 \mu_0 H_{sxy}.$$

In the time domain, these become

$$\mu_0 \frac{\partial H_{sxz}}{\partial t} + \sigma_x \frac{\mu}{\varepsilon} H_{sxz} = -\frac{\partial E_y}{\partial x} - K_{sxz},$$

$$\mu_0 \frac{\partial H_{sxy}}{\partial t} + \sigma_x \frac{\mu}{\varepsilon} H_{sxy} = \frac{\partial E_z}{\partial x} - K_{sxy},$$

$$\frac{\partial K_{sxz}}{\partial t} = \omega_p^2 \mu_0 H_{sxz}, \quad \frac{\partial K_{sxy}}{\partial t} = \omega_p^2 \mu_0 H_{sxy}.$$

The same approach is done for the five remaining equations. We are now in condition to apply Yee's algorithm to the equations

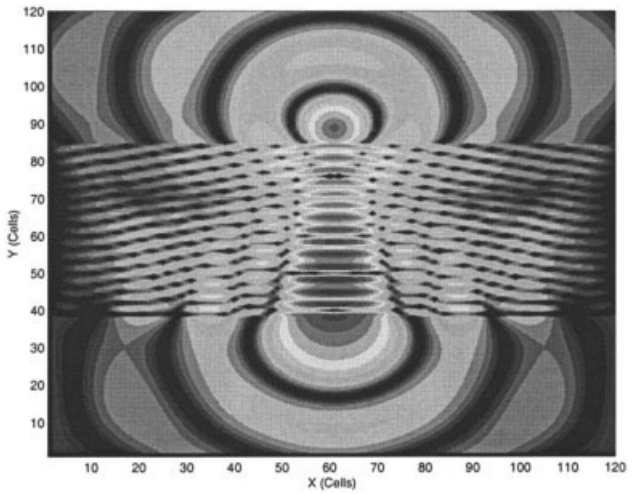

Figure 3 E_z-field intensity distribution at time $t = 1250\Delta t$ for $\omega_p = 500 \times 10^{11}$ rad/s

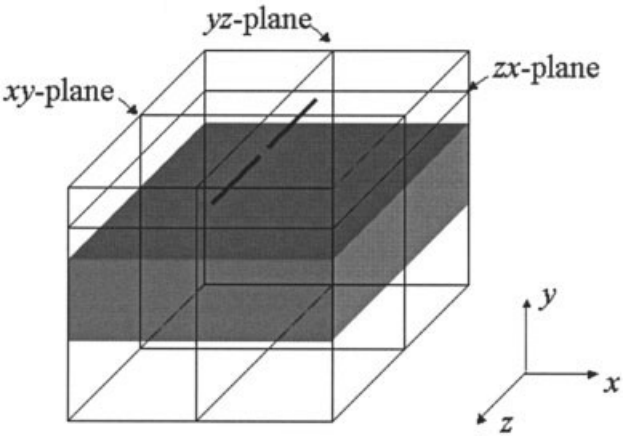

Figure 4 Geometry for the 3D problem with the source in the middle of the dipole

above, with the PML and the Drude model working together in our 3D code.

3. NUMERICAL PARAMETERS

The 3D-FDTD-PML simulator uses the standard leapfrog in time and a regular rectangular grid in space. The magnetic field H as well as its auxiliar current K are located at the cell center, while electric field E and electric current J are located at the cell edge. Then, it requires averaging μ, ε, and σ for E and J. The cell sizes in the simulations below are $\Delta x = \Delta y = \Delta z = 0.025$ cm, corresponding to $\lambda_0/40$ ($f_0 = 30$ GHz). The time step is set to be $\Delta t = 0.95\Delta x/(\sqrt{3}c) = 0.447$ ps. For the PML, we used eight layers with $\sigma_{\max} = 10$. The analytical expression for σ is given by

$$\sigma_u = \sigma_{\max}\left(\frac{u}{L}\right)^2, \tag{5}$$

where u is either x, y, or z and L is the PML's thickness. The expression for the input signal, the same as in [8], is given by

$$f(t) = \begin{cases} g_{\text{on}}(t)\sin(\omega_0 t) & \text{for} \quad 0 \le t < mT_p \\ \sin(\omega_0 t) & \text{for} \quad mT_p \le t < (m+n)T_p \\ g_{\text{off}}(t)\sin(\omega_0 t) & \text{for} \quad (m+n)T_p \le t < (m+n+m)T_p \\ 0 & \text{for} \quad (m+n+m)T_p \le t \end{cases}, \tag{6}$$

where $T_p = 1/f_0$ is the period of one single cycle and the three-derivative smooth window functions are given by

$$g_{\text{on}}(t) = 10x_{\text{on}}^3 - 15x_{\text{on}}^4 + 6x_{\text{on}}^5,$$

$$g_{\text{off}}(t) = 1 - [10x_{\text{off}}^3 - 15x_{\text{off}}^4 + 6x_{\text{off}}^5],$$

with $x_{\text{on}} = 1 - (mT_p - t)/mT_p$ and $x_{\text{off}} = [t - (m+n)]/mT_p$.

The input signal and its frequency components are shown in Figure 1. Clearly, the frequency components are centered at $f_0 = 30$ GHz with the higher and lower frequencies having relative small amplitudes when compared to the target frequency, as expected.

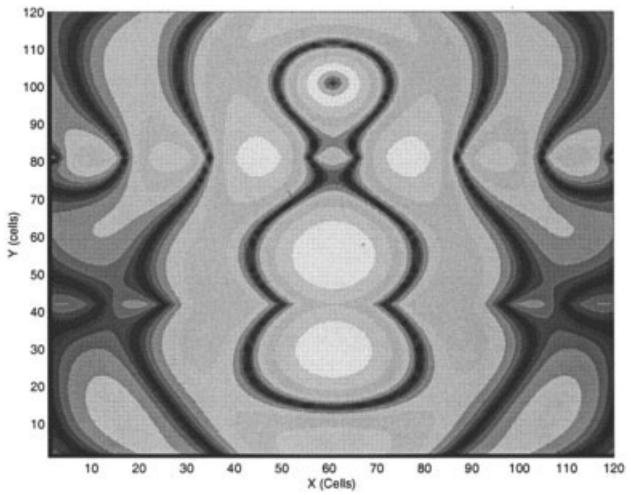

(a)

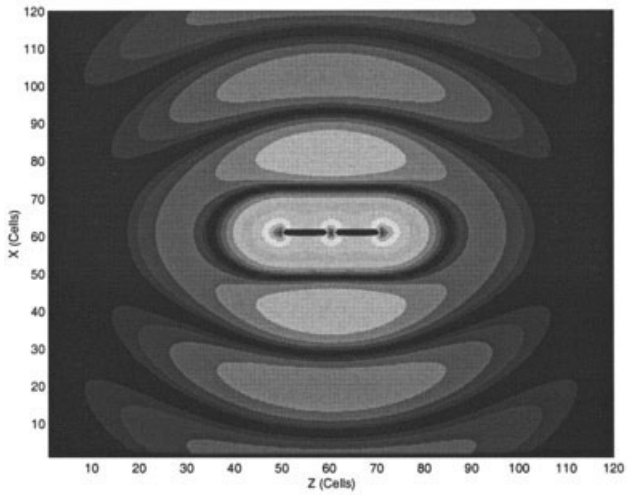

(b)

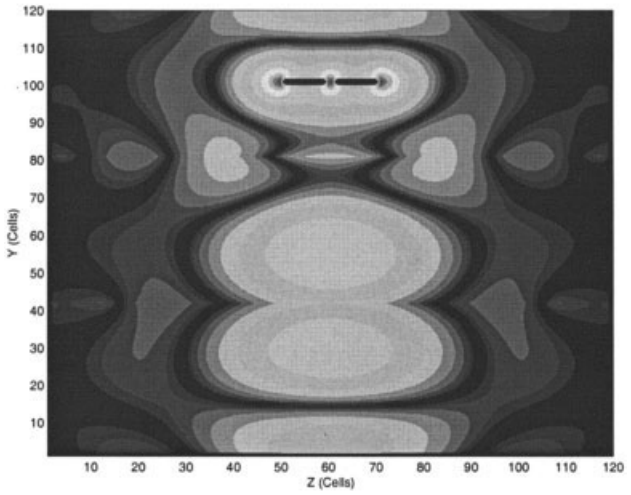

(c)

Figure 5 Field distribution for $\omega = 266 \times 10^{11}$ rad/s in the (a) xy-plane; (b) zx-plane; (c) yz-plane

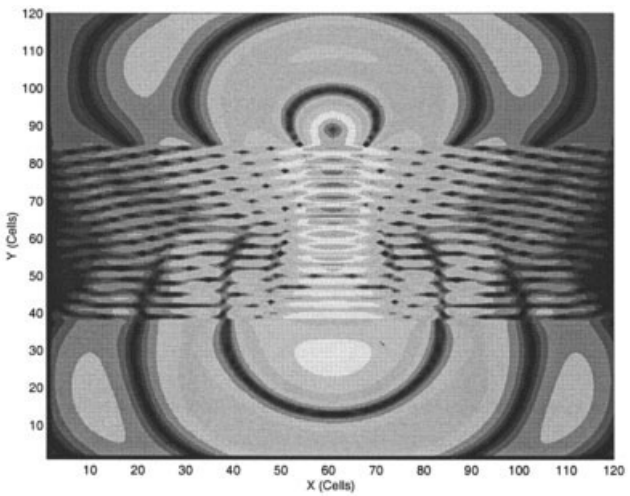

(a)

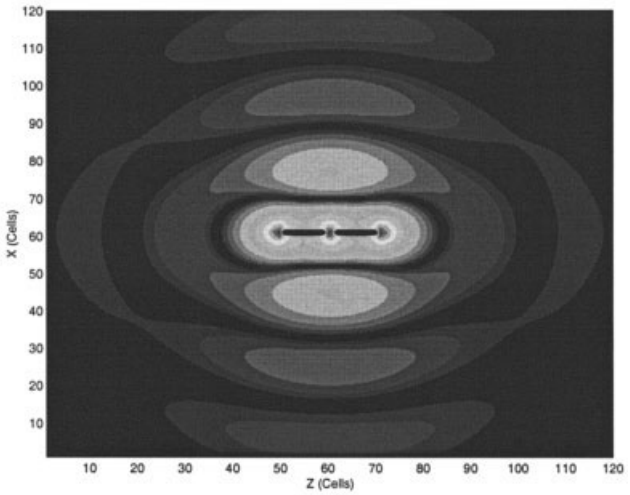

(b)

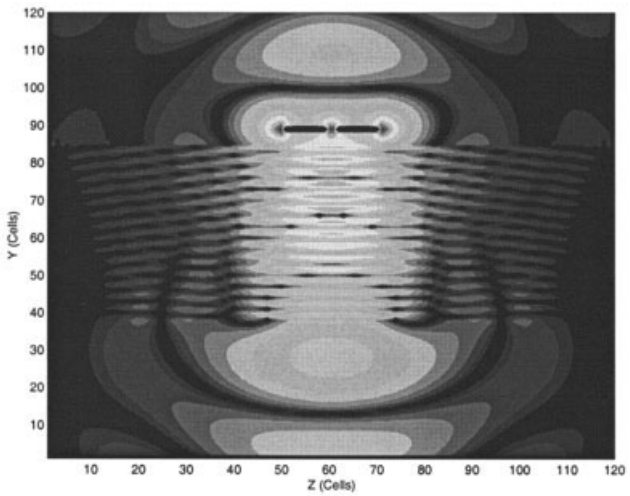

(c)

Figure 6 Field distribution for $\omega = 500 \times 10^{11}$ rad/s in the (a) xy-plane; (b) zx-plane; (c) yz-plane

4. RESULTS

4.1. Comparison with 2D Results

To test our code, we simulate the same problem as [8], used there to check focus properties of LHM. The problem consists of an infinitely long line source located $\lambda_0/2$ above an LHM slab with thickness $d = \lambda_0/2$, which is surrounded by free space. The LHM slab was located exactly in the middle of our domain, occupying $x = [0\ 120]$, $y = [40\ 80]$, and $z = [0\ 30]$ cells, including the PML region. The line source was located at (60, 100, [0 30]), 20 cells away from the slab and the resonant frequency used for expression (3) was set to be $\omega_p = 266.6 \times 10^{11}$ rad/s, which gives $\varepsilon_r = \mu_r \simeq -1$. The computational domain for this example is $120 \times 120 \times 30$ grid points, in the x, y, and z directions, respectively. With the PML approach, we were able to reproduce the results in [8] in a much smaller domain. Figure 2 shows the E_z-field distribution corresponding to the time $t = 1250\Delta t$. The field is shown down to 40 dB below its maximum. In order to compare our simulation to [8], we did not place a PML layer on the front and back faces, perpendicular to the z axis, in the 2D simulations. It should be noted that the field distribution is the same as in Fig. 7 in [8], even with a different precision due to larger time steps and larger cell sizes in our simulation. The same field distribution is also seen in [12].

Another simulation was done in comparison with Fig. 8 in [8]. In this case, the slab is located in the region ([0 120], [36 80], [0 30]), the line source at (60, 88, [0 30]), and $\omega_p = 500 \times 10^{11}$ rad/s. The field is plotted down to 40 dB below its maximum and at a time $t = 1250\Delta t$. As shown in Figure 3, paraxial foci are located at the center of the slab and at the opposite side from the source.

4.2. 3D Simulation of a λ/2 Dipole

Finally, we apply our code to 3D problems. The problem is to simulate a $\lambda_0/2$ dipole $\lambda_0/2$ above an LHM slab with thickness $d = \lambda_0/2$. We reproduced similar geometry to the 2D problems, but with a finite line source. The computational domain for all 3D examples has $120 \times 120 \times 120$ grid points. Figure 4 illustrates the problem's geometry, with the xy-plane cutting at the middle of our domain and the yz- and zx-planes cutting along the dipole. All the fields are plotted down to 60 dB below their maxima.

For the first example, the dipole was located at (60, 100, [−10 10]) with the source at its center, 20 cells away from the slab placed at ([0 120], [40 80], [0 120]) and $\omega_p = 266.6 \times 10^{11}$ rad/s. The field distribution in each plane is shown in Figure 5.

For the second example, the dipole was located at (60, 88, [−10 10]) with the source at its center, four cells away from the slab placed at ([0 120], [36 84], [0 120]) and $\omega_p = 500 \times 10^{11}$ rad/s. The field distribution in each plane is shown in Figure 6.

For all the examples presented here, the colored animation can be found at http://iris-lee3.ece.uiuc.edu/~jjin/jin_home.html, where the wave propagation and focus property are shown more clearly.

5. CONCLUSION

A complete 3D formulation, adding the PML approach to the previous formulation of the Drude medium model, has been developed in this paper. The simulation results show good accuracy as compared to the previously published results. The phenomenon of backward-wave propagation can now be analyzed in any arbitrary direction inside an LHM and more complex and realistic structures can be simulated with our code.

REFERENCES

1. V.G. Veselago, The electrodynamics of substances with simultaneously negative values of ε and μ, Soviet Phys Uspekhi 10 (1968), 509–515.
2. J.P. Pendry, A.J. Holden, D.J. Robbins, and W.J. Stewart, Low-frequency plasmons in thin-wire structures, J Phys Condens Matter 10 (1998), 4785–4809.
3. J.P. Pendry, A.J. Holden, D.J. Robbins, and W.J. Stewart, Magnetism from conductors and enhanced nonlinear phenomena, IEEE Trans Microwave Theory Tech 47 (1999), 2075–2084.
4. R.A. Shelby, D.R. Smith, and S. Schultz, Experimental verification of a negative index of refraction, Sci 292 (2001), 77–79.
5. P.M. Valanju, R.M. Valser, and A.P. Valanju, Wave refraction in negative-index media: Always positive and very inhomogenous, Phys Rev Lett 88 (2002).
6. N. Garcia and M. Nieto-Vesperinas, Left-handed materials do not make a perfect lens, Phys Rev Lett 88 (2002).
7. J. B. Pendry, Negative refraction makes a perfect lens, Phys Rev Lett 85 (2000), 3966–3969.
8. R.W. Ziolkowski and E. Heyman, Wave propagation in media having negative permittivity and permeability, Phys Rev E 64 (2001).
9. R.W. Ziolkowski, Superluminal transmission of information through an electromagnetic matematerial, Phys Rev E 63 (2001).
10. K.S. Yee, Numerical solution of initial boundary value problems involving Maxwell's equations in isotropic media, IEEE Trans Antennas Propagat 14 (1966), 302–307.
11. J.P. Berenger, A perfectly matched layer for the absorption of electromagnetics waves, J Comput Phys 114 (1994), 185–200.
12. M.K. Karkkainem and S.I. Maslovski, Wave propagation, refraction, and focusing phenomena in Lorentzian double-negative materials: A theoretical and numerical study, Microwave Opt Technol Lett 37 (2003), 4–7.

PROPOSED OCDMA ENCODERS AND DECODERS BASED ON SILICA-ON-SILICON INTEGRATED OPTICS

Jian-Guo Zhang,[1] Yumei Wen,[2] and Ping Li[2]

[1] Telecommunications and Internet Engineering Division
School of Engineering, South Bank University
103 Borough Road
London Southern 0AA, UK

[2] Optoelectronic Engineering College
Chongqing University
Chongqing 400044, P.R. China

Received 17 July 2003

ABSTRACT: *A new scheme is proposed for fixed and tunable optical code-division multiple-access (OCDMA) encoders and decoders, which can be implemented by using silica-on-silicon integrated optics to achieve both low loss and compactness. The feasible architectures for OCDMA encoder/decoder are discussed, and the conceptual design is also presented.* © 2004 Wiley Periodicals, Inc. Microwave Opt Technol Lett 40: 205–209, 2004; Published online in Wiley InterScience (www.interscience.wiley.com). DOI 10.1002/mop.11329

Key words: *optical code-division; multiple-access encoders; optical communications; integrated optics*

This work was supported by the Key Laboratory of Optoelectronic Technology & Systems of the State Ministry of Education at the Chongqing University (China) and the Engineering & Physical Sciences Research Council (UK).